ACS OMEGA

Open Access

http://pubs.acs.org/journal/acsodf

Article

Sustained Release Studies of Metformin Hydrochloride Drug Using Conducting Polymer/Gelatin-Based Composite Hydrogels

Aleena Mir, Wilbert J. Fletcher, Darlene K. Taylor, Javed Alam, and Ufana Riaz*

Cite This: *ACS Omega* 2024, 9, 18766−18776

Read Online

ACCESS | Metrics & More | Article Recommendations | Supporting Information

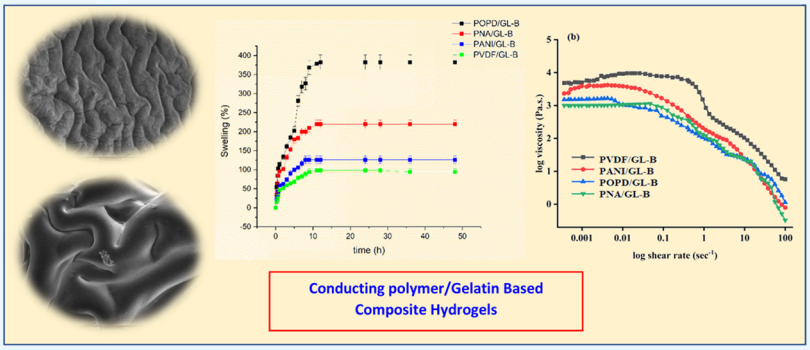

ABSTRACT: The present work highlights the synthesis and characterization of conducting polymer (CP)-based composite hydrogels with gelatin (GL-B) for their application as drug delivery vehicles. The spectral, morphological, and rheological properties of the synthesized hydrogels were explored, and morphological studies confirmed formation of an intense interpenetrating network. Rheological measurements showed variation in the flow behavior with the type of conducting polymer. The hydrogels showed a slow drug release rate of about 10 h due to the presence of the conducting polymer. The release kinetics were fitted in various mathematical models and were best fit in first order for PNA-, POPD-, and PANI-based GL-B hydrogels, and the PVDF/GL-B hydrogel was best fit in the zero-order models. The drug release was found to follow the order: POPD/GL-B > PANI/GL-B > PVDF/GL-B.

INTRODUCTION

Hydrogels have great appeal for a broad range of medical applications, including the release of therapeutic substances such as drugs, proteins etc., due to their soft structure, water absorption, biocompatibility, low surface tension causing low adsorption of proteins, and similarity to the structure of gelatins and biodegradeable polymers.[1−6] Hydrogels make attractive scaffold materials as they have structural resemblance to the extracellular matrix found in many tissues, the ease with which they may be manufactured, and the possibility of minimally invasive delivery.[7]

Conducting polymers (CPs) are organic materials that share traits of metals, along with exceptional qualities of traditional polymers, such as processing flexibility, lightweight, and ease of synthesis.[8−15] For electrically responsive drug delivery, CPs are viewed as potential candidates because they enable distribution in response to electrochemical and/or electrical stimuli as they possess a conjugated system, which enables electron transport through a delocalized pathway.[16,17] Redox processes allow for the control of the charge along the polymer backbone.[18] The reduction−oxidation (redox) state of CPs can be used to control their ability to bind and release charged molecules from their backbones through electrostatic interactions. CPs can therefore be used to deliver the drug at targeted sites through activation of polymer carriers to promote volumetric changes, charge-mediated regulation of drug transport, leading to drug extraction/formation of ionic concentration gradients.[19] As a result, numerous CP-based systems have been developed for the active regulation of drug release.

Enabling both temporally and spatially regulated medication releases using CPs is a significant step toward expanding the clinical impact of implanted drug delivery platforms as these materials exhibit changes in response to factors like solvent, electric field, temperature, pH, light, ionic strength, and external stress.[20−23] Currently, CP-based hydrogels have been used to deliver ketoprofen,[24] anticancer drug,[25−27] and proteins,[28] in gene delivery,[29] and in wearable biosensors.[30] Gelatin (GL) that contains a higher concentration of pyrrolidines produces gels that are more robust. GL can be

Received: July 14, 2023
Revised: August 27, 2023
Accepted: January 10, 2024
Published: April 16, 2024

of type A, which is obtained upon acid treatment, while type B is formed upon treatment with base. GL-B has an isoelectric point (pI) that ranges between 4.8−5.4, and that of GL-A is between 8−9.[31−33] GL is biodegradable and biocompatible, exhibits nonimmunogenic and low antigenicity with harmless product formation on degradation, and shows superior biological performance as compared to other biopolymers.[34−37]

To study the effect of conducting polymers as cross-linkers in enhancing the gelation characteristics of GL-B with a view to improve its drug delivery efficiency, we have synthesized composite hydrogels of GL-B with polyaniline (PANI), poly(*o*-phenylenediamine) (POPD), poly(1-naphthylamine) (PNA), and poly(vinylidene fluoride) (PVDF). The polymers were chosen based on their redox characteristics, which have shown to effectively deliver drugs to the targeted site.[16−19] To the best of our knowledge, there have been no reports on the design of GL-B with CPs for drug release studies.[18] Metformin hydrochloride (MFH) was chosen as a model antidiabetic drug as it is widely utilized to treat diabetes through accelerated peripheral glucose elimination that does not result in hypoglycaemia and therefore makes it popular antidiabetic medication.[38−40] However, with a comparatively short plasma half-life of 1.5−4.5 h, the drug has an absolute bioavailability of 50−60%, and therefore, patient compliance requires frequent administration when higher doses are needed.[41,42] For a once-daily administration of MFH, a formulation that would keep plasma concentration of the drug stable for 10−16 h is desirable.[41] The synthesized composite hydrogels were investigated for their spectral, morphological, and rheological properties via FTIR, UV−visible, SEM, and rheometric techniques. The release kinetics were fitted in various mathematical models to explore the best suited release profiles.

EXPERIMENTAL SECTION

Materials and Methods. *o*-Phenylenediamine (SD Fine Chem. Pvt. Ltd., India), aniline (Merck, India), polyvinylidene fluoride (PVDF), 1-naphthylamine (Merck, India), DMSO (Merck, India), potassium dihydrogen phosphate (Merck, India), ferric chloride (Merck, India), gelatin-B (GL-B) (Sigma-Aldrich), glutaraldehyde (Merk, India), and metformin hydrochloride (MFH) were purchased from Franco-Indian Pharmaceutical Pvt. Ltd., India.

Synthesis of the POPD/GL-B Hydrogel via In Situ Polymerization. Gelatin-B (GL-B) (100 mg) was dissolved in water/methanol (1:1 ratio, 25/25 mL) in a 50 mL beaker and stirred on a magnetic stirrer equipped with N_2 and a thermometer. The monomer o-phenylenediamine (3.2×10^{-2} M, 0.35 g) was added to the GL-B solution followed by the addition of ferric chloride (3.2×10^{-2}, 0.52 g) and kept on stirring for 3 h. The color changed from brown to dark red, confirming the polymerization of o-phenylenediamine monomers. The synthesized hydrogel was washed several times with distilled water so as to remove any unreacted monomer and also to remove any unreacted Fe^{3+} ions. The precipitates were then collected, centrifuged, and dried at 65 °C in a vacuum oven for 72 h. A similar procedure was adopted to synthesize PNA-, PANI-, and PVDF-based gelatin hydrogels. The hydrogel films were prepared by taking 10 mg/mL of the composite hydrogel dispersed in water (10 mL) followed by the addition of glutaraldehyde (0.2M, 5 μL) that resulted in gelation in about 5 min. The synthesized hydrogel films were denoted as POPD/GL-B, PANI/GL-B, PNA/GL-B, and PVDF/GL-B.

Preparation of MFH Drug-Loaded Hydrogels. For the preparation of MFH drug-loaded hydrogels, 10 mg/mL of the composite hydrogel was dispersed in water (100 mL) and subjected to sonication for 30 min followed by the addition of MFH drug (50, 30, 10 mg). Glutaraldehyde (0.2M, 5 μL) was then added to the solution and stirred for 30 s. The hydrogels loaded with drug were then spread on a Petri dish and left overnight at 25 °C. The synthesized hydrogels were thoroughly rinsed with water to remove any unreacted polymer or drug the system. The hydrogel with different concentrations of drugs were denoted as POPD/GL-B-50, POPD/GL-B-30, POPD/GL-B-10, PANI/GL-B-50, PANI/GL-B-30, PANI/GL-B-10, PNA/GL-B-50, PNA/GL-B-30, PNA/GL-B-10, PVDF/GL-B-50, PVDF/GL-B-30, and PVDF/GL-B-10 as per drug loading.

CHARACTERIZATION

Swelling Studies. To optimize the delivering conditions for a controlled drug release of drug molecules, it is helpful to know how much the composites swell. The dry hydrogels were allowed to swell in phosphate buffer (pH 7.4) at 37 °C. The weight of the dehydrated hydrogels was taken as W_o. To measure the hydrated hydrogel, the gels were removed from the receptacle at set intervals. The excess water was removed from the gel surfaces using Whatman filter paper until an equilibrium swelling ratio was obtained. The experiments were performed in triplicate.

$$\text{Swelling ratio} = \frac{(W_s - W_d)}{W_d} \times 100$$

where P_s = percentage swelling, W_s = weight of hydrogel after swelling, and W_d = weight of hydrogel before swelling.

Spectral Studies. The IR spectra of the hydrogel films were recorded using an FTIR spectrophotometer (Shimadzu, Model IRA, Affinity-1) within the range of 450−4000 cm^{-1}.

Morphological Studies. The internal morphology of hydrogels was determined using scanning electron microscopy using a Zeiss 1450EP scanning electron microscope (Carl Zeiss Micro Imaging, Inc., NY).

Rheological Measurements. The prepared hydrogels were examined for their rheological properties using a rheometer (MCR102, Anton Paar, Austria) having a Peltier temperature control system and an accuracy of ±0.01 °C. All the tests were performed at 37 °C. To study the flow properties and viscoelastic behavior of the hydrogels, steady shear tests (γ = 0.001−1000 s^{-1}), amplitude sweep tests (γ = 0.1−100%) at a constant frequency of 5 rad/s, and frequency sweep tests (0.1−100 Hz) at a constant strain of 0.5 were performed.

In Vitro Drug Release Studies. The in vitro drug release studies of MFH-loaded hydrogels were carried out in a USP type II dissolution instrument (LABINDIA) at a rotational speed of 50 rpm.[43−45] A pH of 7.4 was employed in the dissolution media. The dissolution media were prepared by mixing NaOH (9.38 g) and KH_2PO_4 (40 g) in deionized water, respectively, in 1.95 and 2.5 L. The pH was measured using digital pH meters (a pH instructor from EUTECH instrument). The dissolving media were maintained at a temperature of 37.5 °C, and the dissolution media compartment was sealed to eliminate media loss due to evaporation.

https://doi.org/10.1021/acsomega.3c05067
ACS Omega 2024, 9, 18766−18776

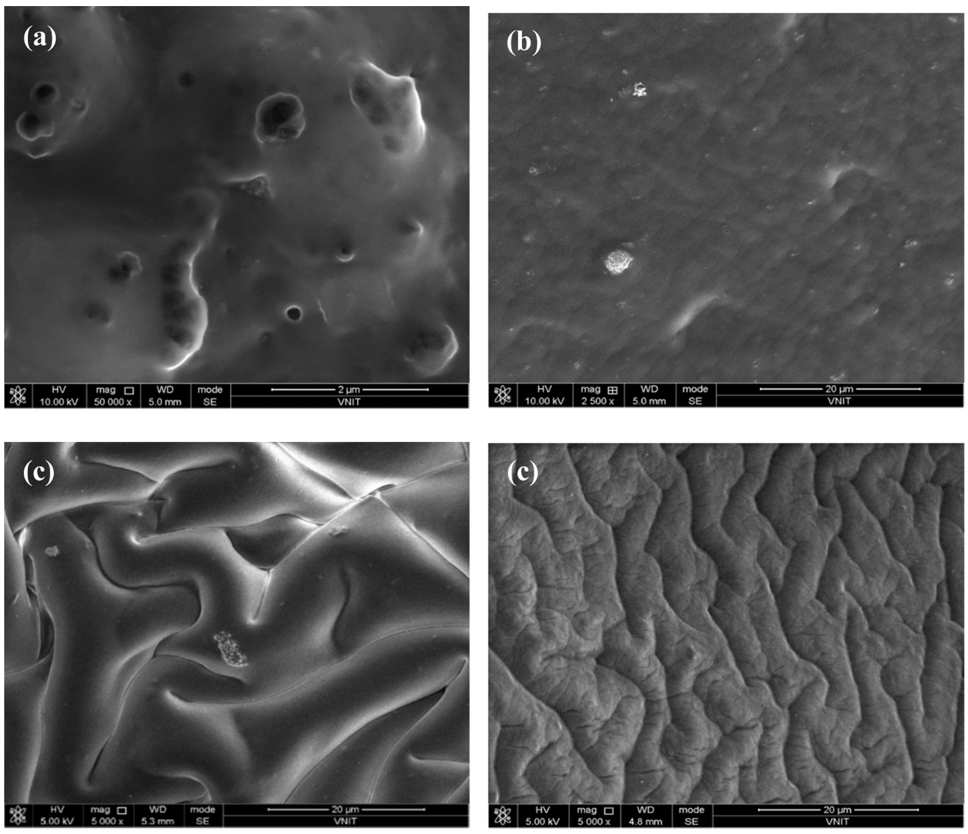

Figure 1. SEM images of (a) POPD/GL-B, (b) PNA/GL-B, (c) PVDF/GL-B, and (d) PANI/GL-B composite hydrogels.

To preserve the sink condition, 5 mL of the solution was taken out of the dissolving device every hour and replaced with a fresh medium. Upon sample collection, each sample was filtered and the drug concentration of each sample was calculated by measuring its absorbance at 225 nm with a UV spectrophotometer model SHIMADZU UV-1800. The following equations were used to evaluate the drug concentration and cumulative drug release:

Concentration of drug (μg/mL) = (slope × absorbance ± intercept)[45]

$$\text{amount of drug release} = \frac{\text{concentration} \times \text{dissolution bath volume} \times \text{dilution factors}}{1000}$$

where the amount of drug release is calculated in mg/mL

$$\text{cumulative percent release \%} = \frac{\text{volume of sample withdrawn (mL)} \times p(t-1) + P_t}{\text{bath volume}}$$

where p_t = percentage release at time t

where p $(t-1)$ = percentage release previous time t[46]

The drug release kinetic was calculated by employing various drug release models: first-order release model $\log C = \log C_0 + \frac{kt}{2.303}$, zero-order release model $Q_t = K_0 t$, Higuchi's model $Q_t = K_h t^{1/2}$, and Korsmeyer–Peppas model $\frac{Q_t}{Q\alpha} = K_p t^n$, where C_0 and C are the concentrations of drug initially and at time t, while Q_t and Q_α are the amounts of drug dissolved at time t and at time infinite.

RESULTS AND DISCUSSION

Spectral Studies. All of the hydrogels showed a prominent peak around 3500–2300 cm^{-1}, which confirmed the coupling of NH stretching with free OH and hydrogen bonding (given in the Supporting Information as Figure S1). The peaks between 1600–1700 cm^{-1} were related to C═O stretching vibration. Bending and stretching vibrations of NH and CN were noticed in the region of 1560–1335 cm^{-1}, while the 1240–670 cm^{-1} bands were related to the vibration of the C–N and N–H planes of bound amide. All of the peaks correlated well with the literature values.[47,48] The composite hydrogel of PANI/GL-B revealed a peak at 3037 cm^{-1}, which was the characteristic peak of the C–H vibration of the aromatic benzene of PANI. The vibration of the C═C stretching peak was noticed at 1619 cm^{-1}, whereas the vibration of the symmetric ring stretching band was found at 1402 cm^{-1}. The stretching of the C–N bonds was observed at 1266 cm^{-1}. The presence of electron-delocalized PANI was confirmed by the presence of a strong peak at 1141 cm^{-1}.[49] Furthermore, the C–H stretching in plane bending was found at 1021 cm^{-1}, while the C–H out of plane bending was noticed at 804 cm^{-1}. Major of the characteristic peaks at 710, 1121, 1216, 1330, 1522, and 1598 cm^{-1} and a broad peak around 3000–3500 confirmed the presence of PANI as reported in the literature.[18] In the case of the POPD/GL-B composite hydrogel, characteristic peaks of primary and secondary amine were found between 3200–3500 cm^{-1}. The strong absorption peak at 1519 cm^{-1} was attributed to the C═C stretching vibrations in the benzene ring, and the peak at 1624 cm^{-1} was correlated with the C═N stretching vibration. The peaks at 1340 and 1216 cm^{-1} were attributed to the C–N stretching vibration of the benzene ring. The peaks at 877, 842, and 686 cm^{-1} were

https://doi.org/10.1021/acsomega.3c05067
ACS Omega 2024, 9, 18766–18776

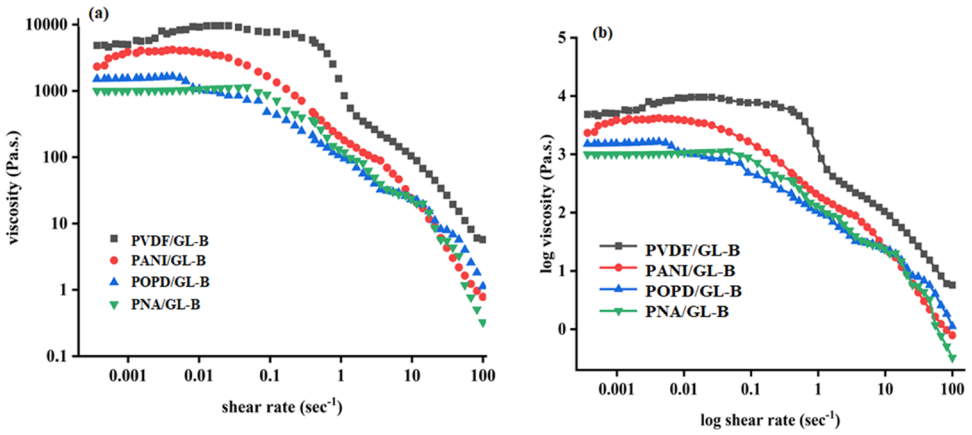

Figure 2. (a) Viscosity as a function of shear rate; (b) log−log plot of the viscosity vs shear rate.

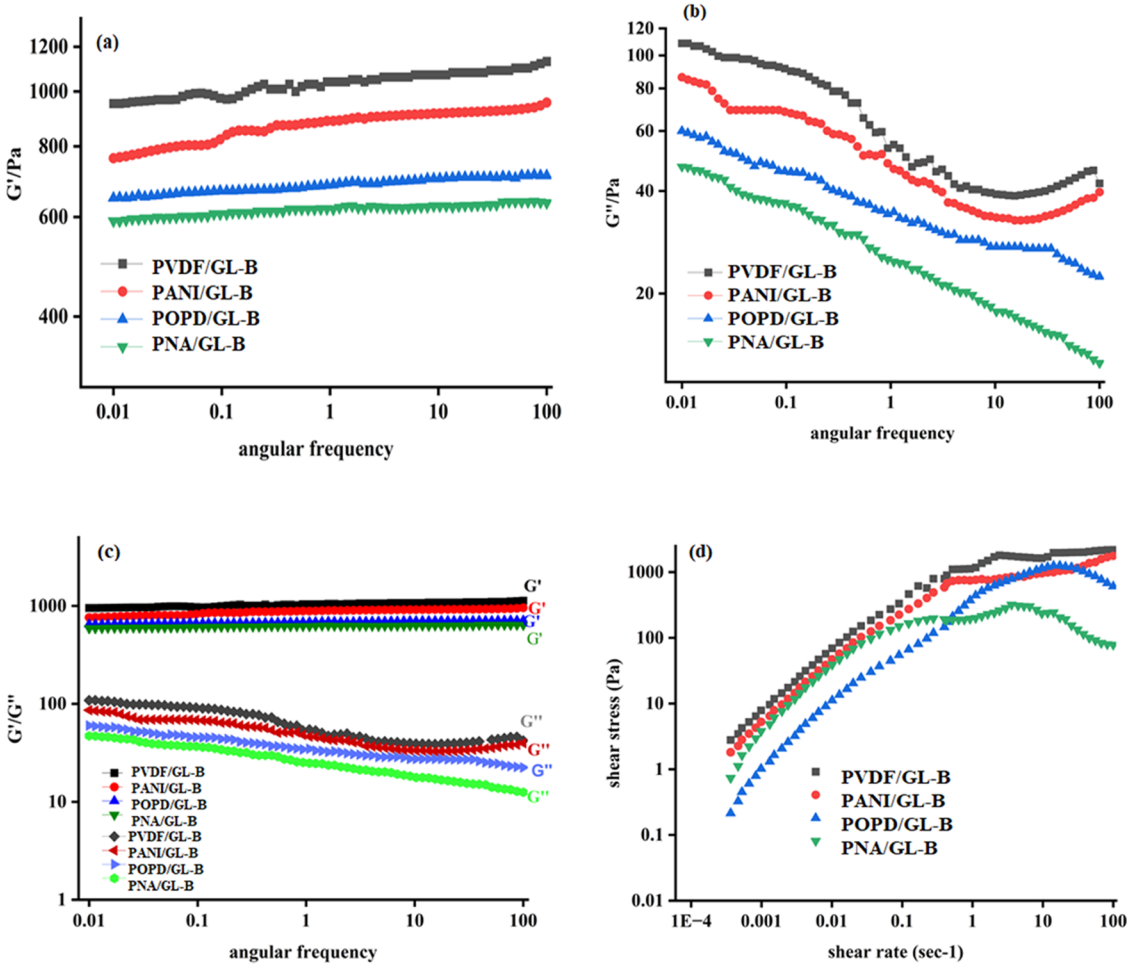

Figure 3. (a) Storage modulus, (b) loss modulus, (c) storage modulus/loss modulus as a function of angular frequency, and (d) flow curve of the shear stress vs shear rate for GL-B-based conducting hydrogels.

correlated with the benzene nuclei in the phenazine skeleton. The quinonoid and benzenoid peaks were found at 1519 and 1492 cm^{-1}, respectively, while the CN stretching peak of the quinonoid and benzenoid units was located at 1216 and 1390 cm^{-1}, respectively. The presence of the NH imine group was confirmed by the presence of a peak at 1624 cm^{-1}. The C═C stretching vibrations in the benzene ring were noticed at 1534 cm^{-1}. In the case of the PNA/GL-B composite hydrogel, the NH-stretching vibration peak was centered at 3481 cm^{-1} for the secondary amine. The imine stretching mode was found at 1641 cm^{-1}, whereas the peak at 1599 cm^{-1} was attributed to the N = Q = N, quinonoid ring skeletal vibrations. The N−B−N benzenoid ring skeletal vibrations appeared at 1529 cm^{-1}, while the CN vibration peaks were noticed at 1401 and 1266 cm^{-1}. The peak at 1151 cm^{-1} was correlated at BNH^{+} = Q and B−NH−B vibrations. The peak at 771 cm^{-1} was compatible with NPA polymerization via N−C (4) links, according to the literature, while the peak at 788 cm^{-1} exhibited N−C (5)

https://doi.org/10.1021/acsomega.3c05067
ACS Omega 2024, 9, 18766−18776

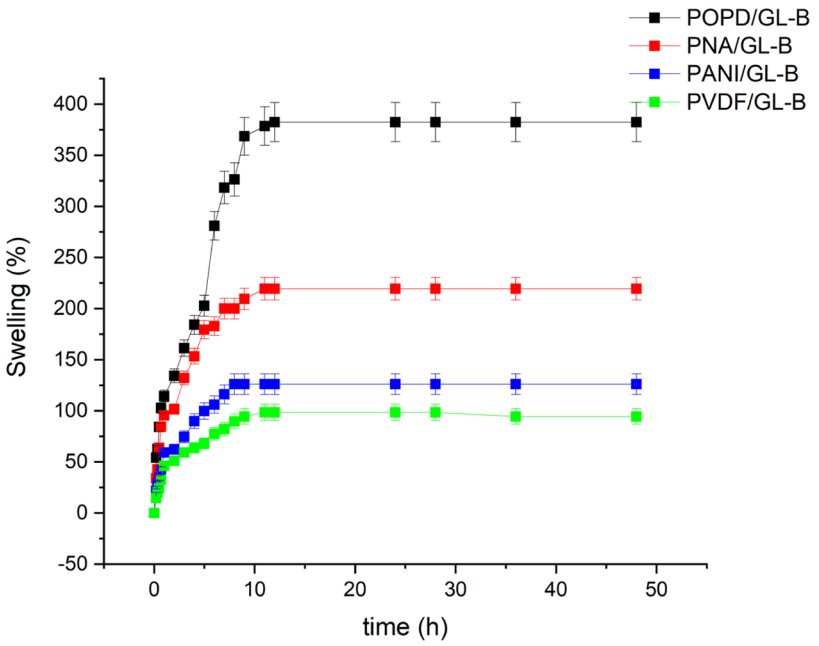

Figure 4. Swelling studies of PNA/GL-B, POPD/GL-B, PANI/GL-B, and PVDF/GL-B composite hydrogels.

coupling between neighboring PNA rings.[48] The baseline's steepness between 2000 and 3000 cm^{-1} confirmed polymerization.[49] The peak at 1630 cm^{-1} in PVDF/GL-B was indicative of the N−N stretching vibration, while the peaks at 1630, 1529, and 841 cm^{-1} were caused by deformation of the N−H vibration. The peak at 1079 cm^{-1} was attributed to the C−H stretching vibration, while the characteristic peaks for the β-phase of PVDF were observed at 510 and 841 cm^{-1}, respectively.[18]

Scanning Electron Microscopy (SEM) Analysis. The SEM image of POPD/GL-B, Figure 1a, showed a swollen gel film with embedded agglomerates, while the SEM image of PNA/GL-B, Figure 1b, exhibited a sheet-like structure showing uniform distribution of PNA in the hydrogel. The SEM image of PVDF/GL-B, Figure 1c, revealed an interwoven layered structure confirming the formation of an interpenetrating network between GL and PVDF.[18] The SEM image of PANI/GL-B, Figure 1d, also showed a uniformly cross-linked network-like morphology having the appearance of stacked sheets. The morphologies showed variation with the type of CP used, which could be utilized to design hydrogels with desired morphologies.

Rheological Studies. Through flow curves of versus shear rate of various conducting hydrogels, the rheological behavior was investigated, Figure 2a,b. The highest viscosity was observed for PVDF/GL-B. As the conducting polymer was varied, the viscosity was also found to be affected. The viscosity of the hydrogels followed the trend PVDF/GL-B > PANI/GL-B> POPD/GL-B > PNA/GL-B. There was a 10^1 fold increase in the viscosity trend with variation of the conducting polymer. Stronger gelation was seen in all cases when the shear rate approached zero, proving that the fluid was not in a state of equilibrium. The hydrogels were discovered to have low, shear-independent viscosities at low shear rates ($\gamma \approx 0.01-0.1\ s^{-1}$), demonstrating yield stress characteristics and conventional Newtonian behavior. The Newtonian behavior and high viscosity may be associated with stabilized hydrogels. However, with an increase in shear rates ($\gamma \approx 10-200\ s^{-1}$), a sharp decline in viscosity was observed, exhibiting a shear thinning region. The decrease in the viscosity was about 4 orders of magnitude, reaching a value of around 10 Pa·s at 10 s^{-1}. This suggested a relatively robust and rigid network structure that prevented gelatin chains from becoming entangled by sliding over one another by forming longer segments from multihelix structures.[17,18] The shear thinning behavior is governed by a number of factors, all of which are related to the structural reorganization of the fluid molecules due to flow. All hydrogels in the Newtonian region exhibited a smaller plateau. The smallest plateau was observed for the POPD/GL-B hydrogel, Figure 2a, while the highest plateau was noticed for PVDF/GL-B. Also, the zero-shear viscosity of all the hydrogels was greater than 10^3 Pa.s. Among all of the hydrogels formed, the POPD/GL-B showed the shortest Newtonian plateau region characterizing liquid-like character of the hydrogel formed. PVDF/GL-B showed an extended plateau region exhibiting solid character of the hydrogel formed. The PANI/GL-B and PNA/GL-B exhibited characteristics similar to that of a solid-like hydrogel. The presence or absence of a Newtonian region indicated the morphology of the gel/air interface, while a flatter interface indicated the presence of a Newtonian region, Figure 2b.

OSCILLATORY FREQUENCY SWEEP MEASUREMENTS

The gels were subjected to an increasing oscillating strain (strain sweep) at a constant frequency. G' (the storage modulus) indicated solid or elastic characters, while G'' (the loss modulus) showed liquid-like/viscous behavior. The oscillatory rheology was measured in the range of angular frequency of 0.01 to 100 rad/s and was plotted for all of the samples. The variation of G' and G'' vs angular frequency for different hydrogels is shown in Figure 3a−c. In the entire region under consideration, the $G' > G''$ showed an increase with an increase in frequency, confirming the stability of composite gel. The hydrogel's nearly independent frequency dependence even at 100 rad/s confirmed that the hydrogels

https://doi.org/10.1021/acsomega.3c05067
ACS Omega 2024, 9, 18766−18776

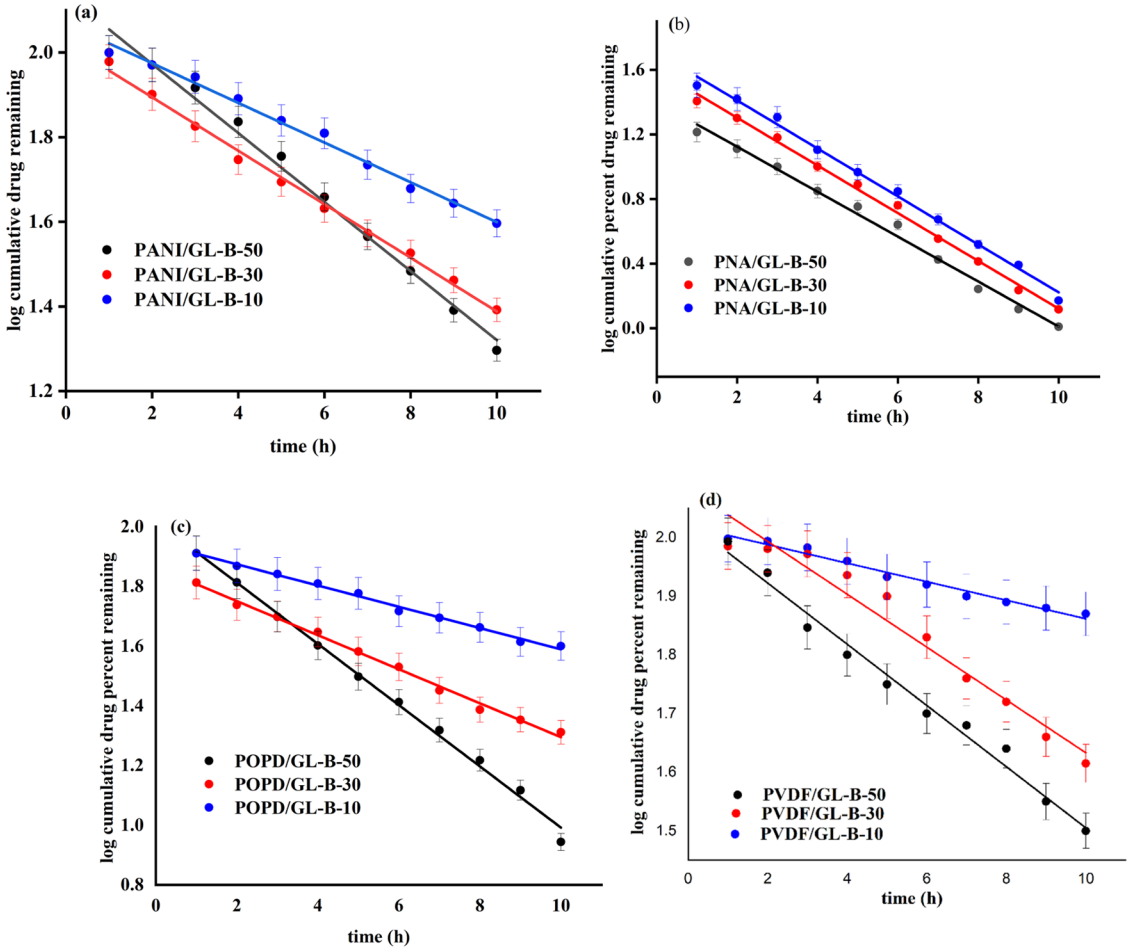

Figure 5. First-order kinetics for (a) PANI/GL-B, (b) PNA/GL-B, and (c) POPD/GL-B and zero order for (d) PVDF/GL-B composite hydrogel.

had a solid network-like arrangement. PVDF/GL-B formed the strongest gel, whereas PNA/GL-B formed the weakest gel. The strength of the hydrogel of PVDF/GL-B ($G' > 10^3$) increases one-fold as compared to that of PNA/GL-B ($G' > 10^2$). Due to the fact that conducting polymers have chains that were positively charged compared to GL-B, which is negatively charged at pH above 5, it can be anticipated that the interaction of these two materials resulted in the formation of electrostatic binding of the conducting polymers to the GL-B chains. The hydrogen bonds also facilitated binding of GL-B with conducting polymers. Among all of the hydrogels formed, PVDF/GL-B showed more solid-like properties and had higher viscosity and G' values indicating a strongly cross-linked network resulting in the highest mechanical strength. The data also demonstrated that the order of zero shear viscosity and value of G' were similar and followed the order PVDF/GL-B > PANI/GL-B > POPD/GL-B > PNA/GL-B. The frequency sweep measurements confirmed that the mechanical stability of the synthesized hydrogels was quite improved as compared to conventional hydrogels, making them an ideal material for drug delivery. The shear stress vs shear rate showed shear thinning behavior for all of the synthesized hydrogels, Figure 3d.

Swelling Studies. Swelling progressed with prolonged immersion exposure and achieved equilibrium after around 12 h, Figure 4. Swelling percent revealed that the highest value was observed for the POPD/GL-B hydrogel at 382%, while the least was observed for PVDF/GL-B at 98%. The highest swelling for the POPD/GL-B hydrogel can be explained by the water loving characteristic of the POPD polymer. The least value for the PVDF/GL-B hydrogel was attributed due to an increase in the cross-link density of the hydrogel. As the cross-linking increased, the ability of the water to penetrate into the hydrogel was significantly decreased, resulting in poor swelling ability for the PVDF/GL-B hydrogel. The reason for swelling of the hydrogel may be due to the polar ionic interaction of the water molecule with the carboxylate group, acidic hydrogen, and conducting polymer. The swelling of the hydrogels followed the order POPD/GL-B > PNA/GL-B > PANI/GL-B > PVDF/GL-B.

In Vitro Release Kinetics of MFH Drug from Composite Hydrogels. The release studies of the MFH drug from composite hydrogels showed a decrease in the absorbance peak corresponding to MFH with time (given in the Supporting Information as Figures S2−S5). The release kinetics of MFH drug from the conducting hydrogels followed zero-order kinetics for PVDF/GL-B, while for PNA/GL-B, POPD/GL-B, and PANI/GL-B composite hydrogels, the release kinetics followed first-order kinetics, Figure 5a−d. The release kinetic studies revealed that as the loading of drug in the hydrogel increased, the concentration of the drug released also increased. PVDF/GL-B showed constant drug release from the matrix. POPD/GL-B revealed the highest drug release, while the PVDF/GL-B exhibited the lowest release, Figure 5d. The highest rate constant for the first-order model was found in the case of POPD/GB-10−50, while the lowest was found in the case of PVDF/GL-B-10.

https://doi.org/10.1021/acsomega.3c05067
ACS Omega 2024, 9, 18766−18776

Table 1. Kinetics Rate Constants and Correlation Coefficient Obtained for the Release of Metformin Hydrochloride Drug Fitted in the Zero-Order Model, First-Order Model, Higuchi Model, and Korsmeyer-Peppas Model

	correlation coefficient (R^2) zero-order model		correlation coefficient (R^2) first-order model		correlation coefficient (R^2) Higuchi model		correlation coefficient (R^2) Korsmeyer-Peppas model	
sample	R^2	k_o	R^2	k_1	R^2	k_h	R^2	k_m
				POPD/GL-B				
POPD/GL-B -50	0.8766	9.2275	0.9955	0.1026	0.9538	41.1314	0.9251	0.9035
POPD/GL-B-30	0.8384	8.6617	0.9950	0.0570	0.9264	38.9087	0.7285	2.2685
POPD/GL-B-10	0.9204	6.5539	0.9940	0.03561	0.9605	28.612	0.7398	2.218
				PNA/GL-B				
PNA/GL-B-50	0.7998	8.5973	0.9915	0.1391	0.8783	38.5014	0.6746	1.4523
PNA/GL-B-30	0.6024	7.0532	0.9959	0.1477	0.7126	32.7834	0.8569	1.8217
PNA/GL-B-10	0.8907	4.9731	0.9950	0.1486	0.88273	21.1565	0.7902	0.8758
				PVDF/GL-B				
PVDF/GL-B-50	0.9911	8.3085	0.9581	0.0465	0.9750	35.1988	0.8972	1.7718
PVDF/GL-B-30	0.9966	7.3890	0.9533	0.0466	0.9753	31.2304	0.8045	2.7081
PVDF/GL-B-10	0.9953	6.3502	0.9186	0.0026	0.9728	26.8212	0.8341	2.5967
				PANI/GL-B				
PANI/GL-B-50	0.9141	9.7106	0.9881	0.08157	0.82314	39.6377	0.9129	3.6189
PANI/GL-B-30	0.9227	9.1535	0.9952	0.06324	0.9416	39.4663	0.8232	2.823
PANI/GL-B-10	0.8936	6.9746	0.9902	0.0469	0.8019	28.4306	0.8693	3.9648

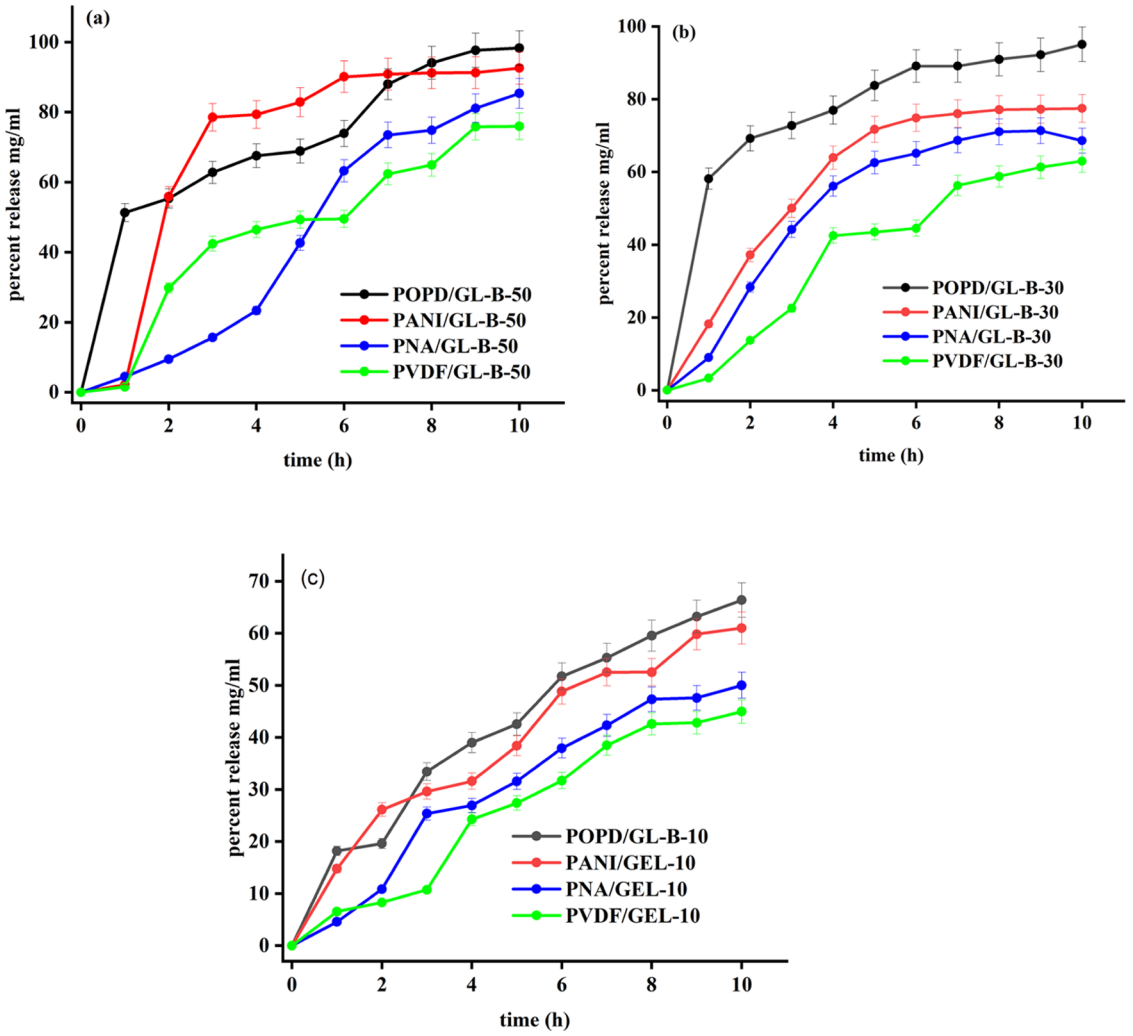

Figure 6. Percent release profiles of conducting polymer/GL-B hydrogels upon loading of (a) 50 mg of MFH drug, (b) 30 mg of MFH drug, and (c) 10 mg MFH drug (pH = 7.4).

https://doi.org/10.1021/acsomega.3c05067
ACS Omega 2024, 9, 18766−18776

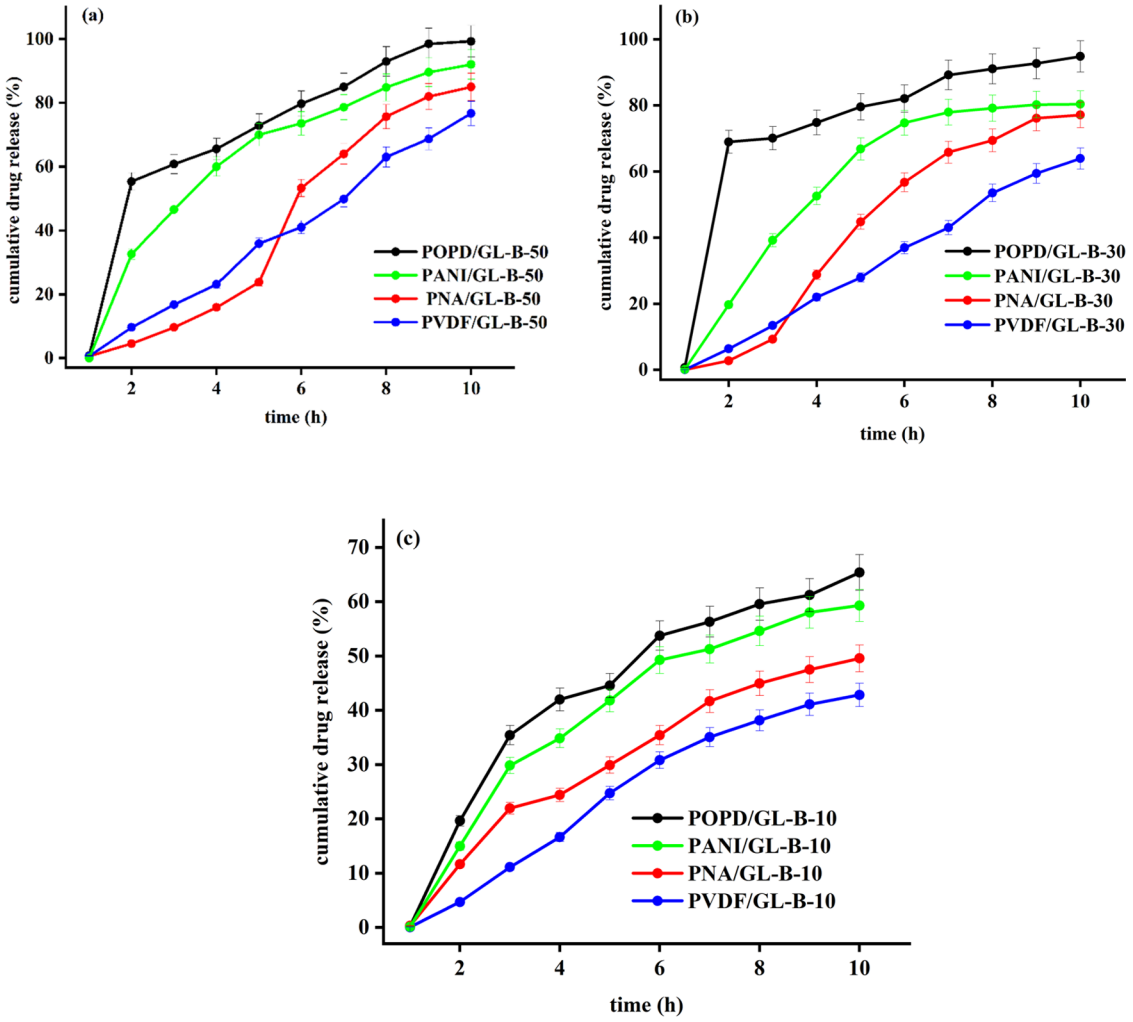

Figure 7. Cumulative drug release profiles of conducting polymer/GL-B hydrogels upon loading of (a) 50 mg of MFH drug, (b) 30 mg of MFH drug, and (c) 10 mg of MFH drug (pH = 7.4).

The rate constant value for zero-order models was the highest in the case of PVDF/GL-B-50 and lowest for PNA/GL-B-10.

Table 1 reveals that, for first-order kinetics, the R^2 value ranged between 0.9881−0.9959 for POPD/GL-B, PNA/GL-B, and PANI/GL-B hydrogels, while for the PVDF/GL-B hydrogel, the value of R^2 ranged between 0.9911−0.996 for zero-order kinetics. The highest rate constant for the first-order model was k_1 = 0.1485 observed for POPD/GL-B -50, while k_1 = 0.0356 was observed for PNA/GL-B-10. For PVDF/GL-B, k_0 = 9.716 for 50 mg of drug loading and k_0 = 6.3502 for 10 mg of drug loading. The release plot in all of the systems demonstrated sustained release behavior. Over the period of 12 h, the % release kinetics of MFH drug via conducting hydrogels were evaluated, Figure 6a−c. The release profile showed that POPD/GL-B-50 released a maximum amount of drug (98.28%), followed by PANI/GL-B-50 (92.58%), Figure 6a.

The hydrogel PVDF/GL-B-10 showed the least drug release (50%) up to 10 h. The drug release percentages for PNA/GL-B-50 and PVDF/GL-B-50 were respectively 85.33 and 75.95%, and for POPD/GL-B-30, the drug release was seen to be the highest, Figure 6b. Drug release from POPD/GL-B-30 and PANI/GL-B-30 was 95.06 and 77.45%, respectively, Figure 6b. For PNA/GL-B-30 and PVDF/GL-B-30 hydrogels, the drug release was found to be 68.605 and 62.98%, respectively. POPD/GL-B-10 showed a drug release of about 66.36%, and PANI/GL-B-10, PNA/GL-B-10, and PVDF/GL-B-10 showed 60.99, 50, and 44.95% release, respectively, Figure 6c. According to the cumulative drug release profile of conducting polymer-based hydrogels, POPD/GL-B-50 released about 100%, whereas PANI/GL-B-50, PNA/GL-B-50, and PVDF/GL-B-50 released 92, 84, and 76%, respectively. The cumulative drug release was at its highest for POPD/GL-B-50, Figure 7a, and at its lowest for PVDF/GL-B-10, Figure 7c. For a 30 mg drug release, Figure 7b, POPD/GL-B-30, PANI/GL-B-30, PNA/GL-B-30, and PVDF/GL-B-30 showed 94, 80, 77, and 63% drug release, respectively, Figure 7b. The drug loading of 10 mg in the same medium showed 65% release for POPD/GL-B-10 and roughly 59% for PANI/GL-B-10, Figure 7c.

Shehata et al.[50] formulated nanoparticles of gelatin/sodium alginate as novel drug administration routes and sustained release qualities. By adjusting the preformulation studies such as flow rate, polymer viscosity, and surface tension, postformulation properties such as particle size, surface scan, and dissolution profiles were evaluated. The studies demonstrated a considerable decrease in blood glucose over the course of 24 h *in vivo* as well as *in vitro* tests. Films made of a chitosan-gelatin hydrogel that contained metformin using

https://doi.org/10.1021/acsomega.3c05067
ACS Omega 2024, 9, 18766−18776

varying genipin concentrations as a cross-linker was synthesized by Ubaid et al.[51] In the first two h of the hydrogel's dissolution in a gastric-simulation environment, burst release was noticed. It was determined that the metformin release rate could be altered by varying the polymer to cross-linker ratio. The release rate was also impacted by the cross-linker; as its concentration increased, it gradually decreased. In ferric chloride solution, sodium alginate (NaAlg)/sodium carboxymethyl cellulose (NaCMC) blend hydrogel beads were synthesized by Swami et *al.*[52] The hydrogel beads that were created showed pH sensitivity during the delivery of metformin hydrochloride. Studies on the in vitro release of drug-loaded beads at pH 7.4 and pH 1.2 revealed different release characteristics. Our recent work on release of metformin drug using Na-alginate-based conducting polymer hydrogels showed that 99% drug release was attained for POPD/Na-ALG at 37 °C over a period of 12 h.[18] Pourjalilia et al.[53] studied the creation of a novel gellan-based magnetic double network hydrogel nanocomposite (MDNH). To examine their drug delivery and mechanical characteristics, samples of Gellan/PAMPS/PAAm DN hydrogels with various concentrations of Fe^{2+}/Fe^{3+} and *N,N′*-methylenebis acrylamide (MBA) components were used to create the cross-linking agents. In vitro release of the drug-loaded hydrogel was investigated at pH 5.4 and pH 7.4. According to the data, lowering the medium pH from 7.4 to 5.4 after 1500 min caused the drug release to increase from 50% at pH = 7.4 to 84% at pH = 5.4. For the immobilization of metformin HCl (MH) at a dose range of 0−30 mg, Hariyanti et al.[54] employed a poly(vinyl alcohol) (PVA)−gelatin-based hydrogel produced by X-ray irradiation with varied gelatin concentrations ranging from 0.5−2% w/v. The total amount of medication released decreased with increasing gelatin concentration and dosage. An in vitro and in vivo toxicity research study of pectin-acrylamide-fabricated hydrogels was used to assess the generated hydrogel by Saramas et al.,[55] which was done using cross-linked *N,N*-methylene bisacrylamide. The proportions of drug release, permeation, and diffusion coefficients were increased with shorter times in comparison to no electrical potential for the drug release permeation of the C 0.8% v/v cryogel via the pig skin. It was demonstrated that the C 0.8% v/v matrix showed the potential to be utilized as a metformin transdermal controlled administration patch for abdominal obesity and diabetes. In our case, the type of conducting polymer greatly influenced the release of the MFH drug from the hydrogel matrix. For the PVDF/GL-B hydrogel, there was a strong interaction observed for fluoride ions of the PVDF polymer and the acidic proton of MFH drug, resulting in very strong interaction of the hydrogel and the drug. This ultimately slowed the release of the drug from the hydrogel matrix. However, in the case of the POPD/GL-B hydrogel, the NH group of the POPD polymer and the NH group of the drug experience strong repulsive forces. This repulsion led to the fast removal of the drug from the POPD-based hydrogel. In the case of the PNA/GL-B hydrogel, the overall attractive forces between the PNA moiety and that of the MFH drug dominated over the repulsive forces, resulting in slower release. The MFH drug loading and various conducting polymers have an impact on the drug release rate. Therefore, by employing a hydrogel based on conducting polymers, the release of drugs from the hydrogel matrix could be appropriately adjusted and controlled for greater performance.

CONCLUSIONS

Conducting hydrogels were successfully synthesized using different conducting polymers blended with gelatin confirmed by FTIR and rheological studies. Incorporation of conducting polymers prolonged the drug release up to 8 h, while gelation provided mechanical and better swelling ability to the hydrogel. Drug release capability of the synthesized hydrogels was examined by loading of metformin hydrochloride at pH = 7.4. The release kinetics of metformin hydrochloride best fit the first-order model. The release data suggested that the drug release from hydrogels depended on the type of conducting polymer and the concentration of drug used. With optimum conducting polymer and drug concentrations, the prolonged release of drug could be achieved, which makes the conducting hydrogels a potential candidate for sustained drug release drug delivery. The in vivo and biocompatibility studies are required for these systems to explore their commercial viability. Moreover, the optimum loading at which the composite could be biodegradable also needs to be investigated. These studies are underway in our laboratory and will be published soon.

ASSOCIATED CONTENT

Supporting Information

The Supporting Information is available free of charge at https://pubs.acs.org/doi/10.1021/acsomega.3c05067.

Figure S1 IR spectra of (a) PNA/GL-B, (b) POPD/GL-B, (c) PANI/GL-B, and (d) PVDF/GL-B, Figure S2 UV-spectra of MFH drug release from (a) PNA/GL-B-50, (b) PNA/GL-B-30, and (c) PNA/GL-B-10 hydrogels, Figure S3 UV-spectra of MFH drug release from (a) POPD/GL-B-50, (b) POPD/GL-B-30, and (c) POPD/GL-B-10 hydrogels, Figure S4 UV-spectra of MFH drug release from (a) PANI/GL-B-50, (b) PANI/GL-B-30, and (c) PANI/GL-B-10 hydrogels, Figure S5 UV-spectra of MFH drug release from (a) PVDF/GL-B-50, (b) PVDF/GL-B-30, and (c) PVDF/GL-B-10 hydrogels (PDF)

AUTHOR INFORMATION

Corresponding Author

Ufana Riaz − *Department of Chemistry and Biochemistry, North Carolina Central University, Durham, North Carolina 27707, United States; Materials Research Laboratory, Department of Chemistry, Jamia Millia Islamia, New Delhi 110025, India;* orcid.org/0000-0001-7485-4103; Email: ufana2002@yahoo.co.in

Authors

Aleena Mir − *Materials Research Laboratory, Department of Chemistry, Jamia Millia Islamia, New Delhi 110025, India;* orcid.org/0000-0002-8402-4469

Wilbert J. Fletcher − *Department of Chemistry and Biochemistry, North Carolina Central University, Durham, North Carolina 27707, United States*

Darlene K. Taylor − *Department of Chemistry and Biochemistry, North Carolina Central University, Durham, North Carolina 27707, United States*

Javed Alam − *King Abdullah Institute for Nanotechnology (KAIN), King Saud University, Riyadh 11451, Saudi Arabia*

Complete contact information is available at: https://pubs.acs.org/10.1021/acsomega.3c05067

https://doi.org/10.1021/acsomega.3c05067
ACS Omega 2024, 9, 18766−18776

Notes

The authors declare no competing financial interest.

■ ACKNOWLEDGMENTS

The corresponding author wishes to acknowledge the Faculty Research Awards Program at NCCU for granting FRAP financial assistance.

■ REFERENCES

(1) Nguyen, Q. V.; Huynh, D. P.; Park, J. H.; Lee, D. S. Injectable polymeric hydrogels for the delivery of therapeutic agents: A review. *Eur. Polym. J.* **2015**, *72*, 602−619.
(2) Radhakrishnan, J.; Krishnan, U. M.; Sethuraman, S. Hydrogel based injectable scaffolds for cardiac tissue regeneration. *Biotechnol. Adv.* **2014**, *32*, 449−461.
(3) Thambi, T.; Li, Y.; Lee, D. S. Injectable hydrogels for sustained release of therapeutic agents. *J. Controlled Release* **2017**, *267*, 57−66.
(4) Mathew, A. P.; Uthaman, S.; Cho, K.-H.; Cho, C.-S.; Park, I.-K. Injectable hydrogels for delivering biotherapeutic molecules. *Int. J. Biol. Macromol.* **2018**, *110*, 17−29.
(5) Riederer, M. S.; Requist, B. D.; Payne, K. A.; Way, J. D.; Krebs, M. D. njectable and microporous scaffold of densely-packed, growth factor-encapsulating chitosan microgels. *Carbohydr. Polym.* **2016**, *152*, 792−801.
(6) Pacelli, S.; Acosta, F.; Chakravarti, A. R.; Samanta, S. G.; Whitlow, J.; Modaresi, S.; Ahmed, R. P. H.; Rajasingh, J.; Paul, A. Nanodiamond-based injectable hydrogel for sustained growth factor release: preparation, characterization and in vitro analysis. *Acta Biomater.* **2017**, *58*, 479−491.
(7) Drury, J. L.; Mooney, D. J. Hydrogels for tissue engineering: scaffold design variables and applications. *Biomaterials* **2003**, *24*, 4337−4351.
(8) Riaz, U.; Ashraf, S. M. Semi-conducting poly (1-naphthylamine) nanotubes: A pH independent adsorbent of sulphonate dyes. *Chem.Eng. J.* **2011**, *174* (2−3), 546−555.
(9) Zia, J.; Kashyap, J.; Riaz, U. Facile synthesis of polypyrrole encapsulated V2O5 nanohybrids for visible light driven green sonophotocatalytic degradation of antibiotics. *J. Mol. Liq.* **2018**, *272*, 834−850.
(10) Riaz, U.; Jadoun, S.; Kumar, P.; Kumar, R.; Yadav, N. Microwave-assisted facile synthesis of poly (luminol-co-phenylenediamine) copolymers and their potential application in biomedical imaging. *RSC Adv.* **2018**, *8* (65), 37165−37175.
(11) Riaz, U.; Ashraf, S. M.; Madan, A. Effect of microwave irradiation time and temperature on the spectroscopic and morphological properties of nanostructured poly(carbazole) synthesized within bentonite clay galleries. *New J. Chem.* **2014**, *38* (9), 4219−4228.
(12) Yadav, A.; Kumar, H. Self-assembled quantum dots decorated polypyrrole based multifunctional nanocomposite. *Colloids Surf., A* **2023**, *666* (5), No. 131241.
(13) Yadav, A.; Kumar, H.; Kumari, R.; Sharma, R. Progress in the development of metal nanoparticles encapsulated with Polypyrrole plastic nanocomposites: Antibacterial and photocatalytic properties. *Mater. Sci. Eng. B* **2022**, *286*, No. 116085.
(14) Kumar, H.; Luthra, M.; Punia, M.; Singh, R. M. Co_3O_4/PANI nanocomposites as a photocatalytic, antibacterial and anticorrosive agent: Experimental and theoretical approach. *Colloid Interface Sci. Commun.* **2021**, *45*, No. 100512.
(15) Yadav, A.; Kumar, H.; Sharma, R.; Kumari, R.; Thakur, M. Quantum dot decorated polyaniline plastic as a multifunctional nanocomposite: experimental and theoretical approach. *RSC Adv.* **2022**, *12*, 24063−24076.
(16) Riaz, U.; Nabi, N.; Nwanze, F. R.; Yan, F. Experimental and biophysical interaction studies of alanine modified polyaniline with bovine serum albumin and human serum albumin: Influence of alanine modification on the spectral, morphological and electronic properties. *Synth. Met.* **2023**, *292*, No. 117248.
(17) Mir, A.; Kumar, A.; Alam, J.; Riaz, U. Synthesis and characterization of pH-responsive, conducting polymer/Na-alginate/gelatin based composite hydrogels for sustained release of amoxicillin drug. *Int. J. Biol. Macromol.* **2023**, *252*, 12601.
(18) Mir, A.; Kumar, A.; Riaz, U. Synthesis and characterization of conducting polymer/alginate composite hydrogels: Effect of conducting polymer loading on the release behaviour of metformin drug. *J. Mol. Liq.* **2023**, *372*, No. 121193.
(19) Riaz, U.; Singh, N.; Srambikal, F. R.; Fatima, S. A review on synthesis and applications of polyaniline and polypyrrole hydrogels. *Polym. Bull.* **2023**, *80* (2), 1085−1116.
(20) Svirskis, D.; Travas-Sejdic, J.; Rodgers, A.; Garg, S. Electrochemically controlled drug delivery based on intrinsically conducting polymers. *J. Controlled Release* **2010**, *146*, 6−15.
(21) Rong, Q.; Lei, W.; Liu, M. Conductive hydrogels as smart materials for flexible electronic devices. *Chem. − A Eur. J.* **2018**, *24*, 16930−16943.
(22) Pyarasani, R. D.; Jayaramudu, T.; John, A. Polyaniline-based conducting hydrogels. *J. Mater. Sci.* **2019**, *54*, 974−996.
(23) Liu, K.; Wei, S.; Song, L.; Liu, H.; Wang, T. Conductive hydrogels—A novel material: Recent advances and future perspectives. *J. Agric. Food Chem.* **2020**, *68*, 7269−7280.
(24) Park, S.-Y.; Kang, J.-H.; Kim, H.-S.; Hwang, J.-Y.; Shin, U. S. Electrical and thermal stimulus-responsive nanocarbon-based 3D hydrogel sponge for switchable drug delivery. *Nanoscale* **2022**, *14*, 2367−2382.
(25) Aslam, M.; Barkat, K.; Malik, N. S.; Alqahtani, M. S.; Anjum, I.; Khalid, I.; Tulain, U. R.; Gohar, N.; Zafar, H.; Paiva-Santos, A. C.; Raza, F. pH Sensitive Pluronic Acid/Agarose-Hydrogels as Controlled Drug Delivery Carriers: Design, Characterization and Toxicity Evaluation. *Pharmaceutics* **2022**, *14*, 1218.
(26) Sankarganesh, P.; Parthasarathy, V.; Kumar, A. G.; Saraniya, M.; Udayakumari, N.; Ragu, S. Development of novel mannitol blended PVA hydrogel membrane and its anticancer and antimicrobial drug delivery potential for wound dressing applications. *J. Sol−Gel Sci. Technol.* **2022**, *103*, 447−456.
(27) Anirudhan, T. S.; Mohan, M.; Rajeev, M. R. Modified chitosan-hyaluronic acid based hydrogel for the pH-responsive Co-delivery of cisplatin and doxorubicin. *Int. J. Biol. Macromol.* **2022**, *201*, 378−388.
(28) Shahbazizadeh, S.; Naji-Tabasi, S.; Shahidi-Noghabi, M. Development of soy protein/sodium alginate nanogel-based cress seed gum hydrogel for oral delivery of curcumin. *Chem. Biol. Technol. Agric.* **2022**, *9*, No. 41.
(29) Attias Cohen, S.; Simaan-Yameen, H.; Fuoco, C.; Gargioli, C.; Seliktar, D. Injectable hydrogel microspheres for sustained gene delivery of antisense oligonucleotides to restore the expression of dystrophin protein in duchenne muscular dystrophy. *Eur. Polym. J.* **2022**, *166*, No. 111038.
(30) Jing, Y.; Wang, A.; Li, J.; Li, Q.; Han, Q.; Zheng, X.; Cao, H.; Bai, S. Preparation of conductive and transparent dipeptide hydrogels for wearable biosensor. *Bio-Des. Manuf.* **2022**, *5*, 153−162.
(31) Oakenfull, D.; Scott, A. Gelatin gels in deuterium oxide. *Food Hydrocolloids* **2003**, *17*, 207−210.
(32) Gómez-Guillén, M.; Giménez, B.; López-Caballero, M. E.; Montero, M. P. Functional and bioactive properties of collagen and gelatin from alternative sources: A review. *Food Hydrocolloids* **2011**, *25*, 1813−1827.
(33) Aramwit, P.; Jaichawa, N.; Ratanavaraporn, J.; Srichana, T. A comparative study of type A and type B gelatin nanoparticles as the controlled release carriers for different model compounds. *Mater. Express* **2015**, *5*, 241−248.
(34) Nezhadi, S. H.; Choong, P. F. M.; Lotfipour, F.; Dass, C. R. Gelatin-based delivery systems for cancer gene therapy. *J. Drug Target.* **2009**, *17*, 731−738.
(35) *Controlled Pulmonary Drug Delivery*; Smyth, H. D. C.; Hickey, A. J., Eds.; Springer New York: New York, NY, 2011.
(36) Elzoghby, A. O. Gelatin-based nanoparticles as drug and gene delivery systems: reviewing three decades of research. *J. Controlled Release* **2013**, *172*, 1075−1091.

https://doi.org/10.1021/acsomega.3c05067
ACS Omega 2024, 9, 18766−18776

(37) Wang, H.; Boerman, O. C.; Sariibrahimoglu, K.; Li, Y.; Jansen, J. A.; Leeuwenburgh, S. C. G. Comparison of micro- vs. nano-structured colloidal gelatin gels for sustained delivery of osteogenic proteins: Bone morphogenetic protein-2 and alkaline phosphatase. *Biomaterials* **2012**, *33*, 8695−8703.
(38) Nasri, H.; Rafieian-Kopaei, M. Metformin: current knowledge. *J. Res. Med. Sci.* **2014**, *19*, 658−664.
(39) Klepser, T. B.; Kelly, M. W. Metformin hydrochloride: an antihyperglycemic agent. *Am. J. Heal. Pharm.* **1997**, *54*, 893−903.
(40) Rösen, P.; Wiernsperger, N. F. Metformin delays the manifestation of diabetes and vascular dysfunction in Goto−Kakizaki rats by reduction of mitochondrial oxidative stress. *Diabetes. Metab. Res. Rev.* **2006**, *22*, 323−330.
(41) Dunn, C. J.; Peters, D. H. Metformin. *Drugs* **1995**, *49*, 721−749.
(42) Defang, O.; Shufang, N.; Wei, L.; Hong, G.; Hui, L.; Weisan, P. In vitro and in vivo evaluation of two extended release preparations of combination metformin and glipizide. *Drug Dev. Ind. Pharm.* **2005**, *31*, 677−685.
(43) Verma, A.; Riaz, U. Spectral, thermal and morphological characteristics of ultrasonically synthesized poly(anisidine-co-phenylenediamine)/bentonite nanocomposites: A potential anti-diabetic drug carrier. *J. Mol. Liq.* **2018**, *261*, 1−13.
(44) Verma, A.; Riaz, U. Sonolytically intercalated poly (anisidine-co-toluidine)/bentonite nanocomposites: pH responsive drug release characteristics. *J. Drug Delivery Sci. Technol.* **2018**, *48*, 49−58.
(45) You, Y.-Z.; Oupický, D. Synthesis of Temperature-Responsive Heterobifunctional Block Copolymers of Poly(ethylene glycol) and Poly(*N*-isopropylacrylamide). *Biomacromolecules* **2007**, *8*, 98−105.
(46) Viseras, C.; Aguzzi, C.; Cerezo, P.; Bedmar, M. C. Biopolymer−clay nanocomposites for controlled drug delivery. *Mater. Sci. Technol.* **2008**, *24*, 1020−1026.
(47) Hashim, D. M.; Man, Y. B. C.; Norakasha, R.; Shuhaimi, M.; Salmah, Y.; Syahariza, Z. A. Potential use of Fourier transform infrared spectroscopy for differentiation of bovine and porcine gelatins. *Food Chem.* **2010**, *118*, 856−860.
(48) Cebi, N.; Durak, M. Z.; Toker, O. S.; Sagdic, O.; Arici, M. An evaluation of Fourier transforms infrared spectroscopy method for the classification and discrimination of bovine, porcine and fish gelatins. *Food Chem.* **2016**, *190*, 1109−1115.
(49) Kang, E. Polyaniline: a polymer with many interesting intrinsic redox states. *Prog. Polym. Sci.* **1998**, *23*, 277−324.
(50) Shehata, T. M.; Ibrahima, M. M. BÜCHI nano spray dryer B-90: a promising technology for the production of metformin hydrochloride-loaded alginate−gelatin nanoparticles. *Drug Dev. Ind. Pharm.* **2019**, *45*, 1907−1914.
(51) Ubaid, M.; Murtaza, G. Fabrication and characterization of genipin cross-linked chitosan/gelatin hydrogel for pH-sensitive, oral delivery of metformin with an application of response surface methodology. *Int. J. Biol. Macromol.* **2018**, *114*, 1174−1185.
(52) Swamy, B. Y.; Yun, Y.-S. In vitro release of metformin from iron (III) cross-linked alginate−carboxymethyl cellulose hydrogel beads. *Int. J. Biol. Macromol.* **2015**, *77*, 114−119.
(53) Pourjalili, N.; Bagheri Marandi, G.; Kurdtabar, M.; Rezanejade Bardajee, G. Synthesis and characterization of double network hydrogel based on gellan-gum for drug delivery. *J. Macromol. Sci., Part A: Pure Appl.Chem.* **2022**, *59*, 537−549.
(54) Hariyanti, H.; Erizal, E.; Mustikarani, E.; Lestari, I.; Lukitowati, F. In Vitro Release of Metformin HCl from Polyvinyl Alcohol (PVA)-Gelatin Hydrogels Prepared by Gamma Irradiation. *At. Indones.* **2022**, *48*, 37.
(55) Saramas, T.; Sakunpongpitiporn, P.; Rotjanasuworapong, K.; Morarad, R.; Niamlang, S.; Sirivat, A. Metformin delivery via iontophoresis based on κ-carrageenan cryogels. *Int. J. Biol. Macromol.* **2022**, *223*, 702−712.

https://doi.org/10.1021/acsomega.3c05067
ACS Omega 2024, 9, 18766−18776